JOURNAL OF GEOPHYSICAL RESEARCH, VOL. 107, NO. B4, 2060, 10.1029/2001JB000202, 2002

# Aftershock triggering by complete Coulomb stress changes

Debi Kilb[1]
Center for Earthquake Research and Information, University of Memphis, Memphis, Tennessee, USA

Joan Gomberg
U.S. Geological Survey, Center for Earthquake Research and Information, Memphis, Tennessee, USA

Paul Bodin
Center for Earthquake Research and Information, University of Memphis, Memphis, Tennessee, USA

Received 20 September 2000; revised 9 February 2001; accepted 21 August 2001; published 11 April 2002.

[1] We examine the correlation between seismicity rate change following the 1992, *M*7.3, Landers, California, earthquake and characteristics of the complete Coulomb failure stress (CFS) changes ($\Delta$CFS($t$)) that this earthquake generated. At close distances the time-varying "dynamic" portion of the stress change depends on how the rupture develops temporally and spatially and arises from radiated seismic waves and from permanent coseismic fault displacement. The permanent "static" portion ($\Delta$CFS) depends only on the final coseismic displacement. $\Delta$CFS diminishes much more rapidly with distance than the transient, dynamic stress changes. A common interpretation of the strong correlation between $\Delta$CFS and aftershocks is that load changes can advance or delay failure. Stress changes may also promote failure by physically altering properties of the fault or its environs. Because it is transient, $\Delta$CFS($t$) can alter the failure rate only by the latter means. We calculate both $\Delta$CFS and the maximum positive value of $\Delta$CFS($t$) (peak $\Delta$CFS($t$)) using a reflectivity program. Input parameters are constrained by modeling Landers displacement seismograms. We quantify the correlation between maps of seismicity rate changes and maps of modeled $\Delta$CFS and peak $\Delta$CFS($t$) and find agreement for both models. However, rupture directivity, which does not affect $\Delta$CFS, creates larger peak $\Delta$CFS($t$) values northwest of the main shock. This asymmetry is also observed in seismicity rate changes but not in $\Delta$CFS. This result implies that dynamic stress changes are as effective as static stress changes in triggering aftershocks and may trigger earthquakes long after the waves have passed. *INDEX TERMS:* 7209 Seismology: Earthquake dynamics and mechanics; 7215 Seismology: Earthquake parameters; 7230 Seismology: Seismicity and seismotectonics; 7260 Seismology: Theory and modeling; *KEYWORDS:* Aftershock triggering, Landers earthquake 1992, Coulomb stress, reflectivity, dynamic stress changes, seismicity rate change

## 1. Introduction

[2] Earthquakes can influence the occurrence of other earthquakes. Aftershock sequences exemplify this type of behavior and provide useful data sets because of their abundance and clear relationship to main shocks. To better understand the phenomenon of earthquake triggering, we examine the correlation between characteristics of the complete Coulomb failure stress (CFS) changes, $\Delta$CFS($t$), caused by a large earthquake and the associated seismicity rate changes in regions usually identified as the aftershock zone.

[3] Coulomb stress changes (defined in section 2.1) can be categorized as static or dynamic [*Harris*, 1998; *Belardinelli et al.*, 1999; *Marone*, 2000; *Voisin et al.*, 2000]. The static Coulomb stress change, $\Delta$CFS, is permanent and depends on the final fault offset, and it is not influenced by the rupture process. The time-varying, transient portions of $\Delta$CFS($t$), or dynamic stress changes, are transmitted via propagating seismic waves. In the near field the static stress change is inseparable from the radiated wave field. Static stress changes diminish much more rapidly with distance from the source than do the deformations associated with the seismic waves (Figure 1).

[4] Numerous recent studies attempt to correlate regions of positive $\Delta$CFS with increased seismic activity and regions of negative $\Delta$CFS with zones of postearthquake quiescence [e.g., *Das and Scholz*, 1981; *Stein and Lisowski*, 1983; *King et al.*, 1994; *Nostro et al.*, 1997; *Hardebeck et al.*, 1998; *Harris*, 1998; *Toda et al.*, 1998; *Anderson and Johnson*, 1999; *Stein*, 1999]. These correlations are surprising because the static stress changes are typically small, often 2 orders of magnitude less than earthquake stress drops. Some studies have concluded that $\Delta$CFS alone cannot promote rupture [e.g., *Harris and Simpson*, 1992; *Bennett et al.*, 1995; *Astiz et al.*, 2000], and other studies have concluded that the relevance of such changes remains unproven [*Du and Aydin*, 1993; *Dodge et al.*, 1995]. At remote distances (i.e., several source dimensions away from the rupture), dynamic stress changes have been associated with triggered earthquakes because they are orders of magnitude larger than $\Delta$CFS [*Hill et al.*, 1993; *Anderson et al.*, 1994; *Gomberg and Bodin*, 1994; *Hill et al.*, 1995; *Gomberg*, 1996; *Gomberg and Davis*, 1996; *Gomberg et al.*, 1997]. It seems reasonable to expect that dynamic stress changes may also trigger nearby aftershocks because the maximum positive value of $\Delta$CFS($t$) (peak $\Delta$CFS($t$)) always equals or exceeds $\Delta$CFS [*Rybicki et al.*, 1985; *Hill et al.*, 1993; *Cotton and Coutant*, 1997; *Belardi-*

[1]Now at Institute of Geophysics and Planetary Physics, University of California, San Diego, La Jolla, California, USA.


0148-0227/02/2001JB000202$09.00

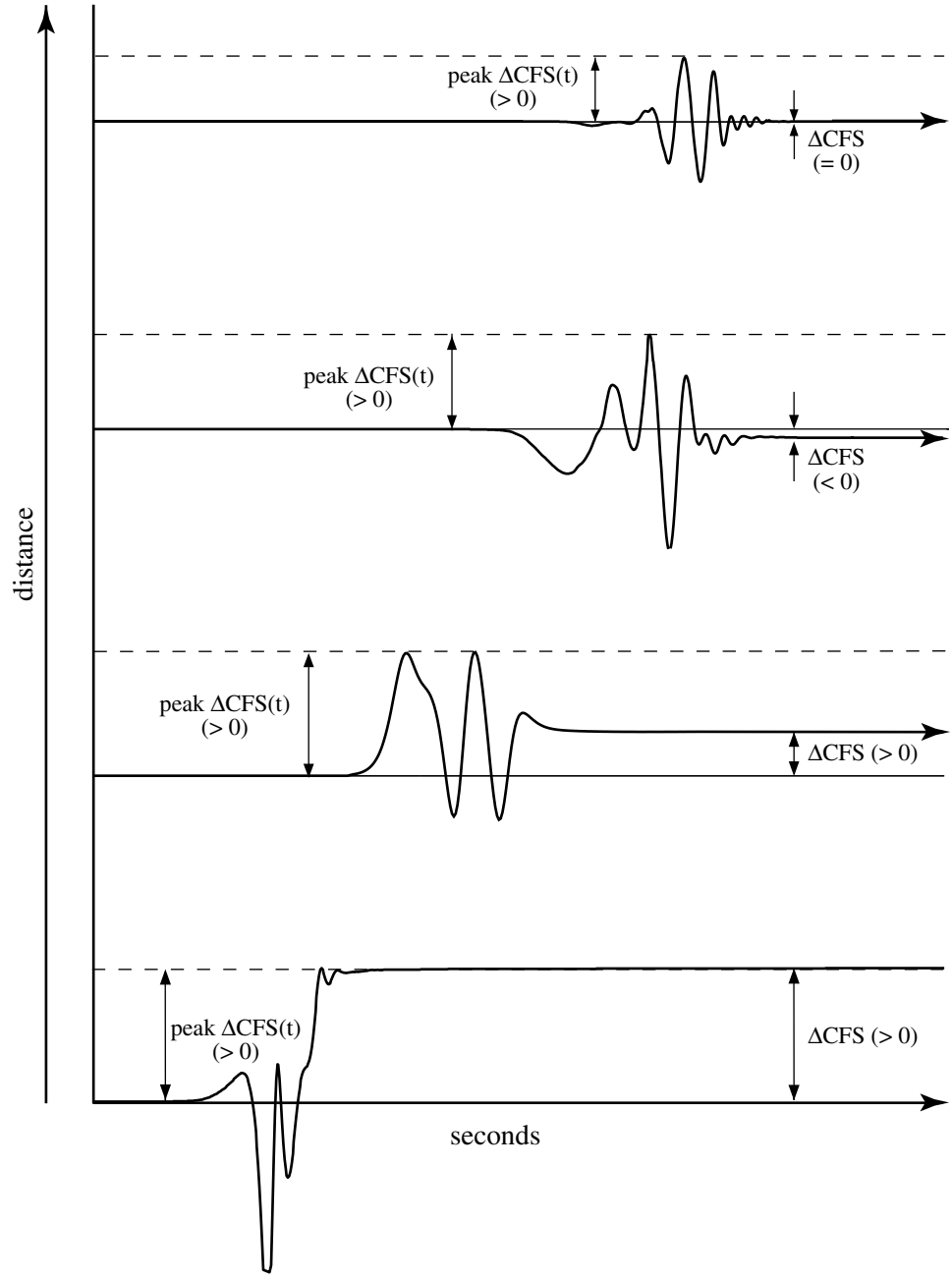


**Figure 1.** Coulomb stress-gram cartoons illustrating peak Coulomb stress change (peak $\Delta$CFS($t$)) and static Coulomb stress change ($\Delta$CFS), and their variation with distance. In the far field, peak $\Delta$CFS($t$) are larger than $\Delta$CFS, but near-field values are comparable. By definition, peak $\Delta$CFS($t$) cannot be negative.

*nelli et al.*, 1999]. At close distances the ratio (peak $\Delta$CFS($t$))/$\Delta$CFS is approximately proportional to the source-receiver distance, $R$, and at larger distances proportional to $R^2$ [*Aki and Richards*, 1980]. Moreover, if dynamic stress changes trigger remote earthquakes, they must also do so at close distances simply because triggered earthquakes have no knowledge of the distance to the causative stress changes.

[5] Coulomb stress changes can influence fault rupture in at least two ways. The first is by raising or lowering the applied accumulating load (e.g., plate tectonic loading); positive $\Delta$CFS enhances the applied load, while negative $\Delta$CFS diminishes it. Dynamic Coulomb stress changes cannot permanently alter the applied load. The second way stress changes might facilitate failure is to modify properties of the fault and/or its immediate environment. Laboratory tests and field observations have shown that changes in a fault's physical properties (e.g., erosion of asperities, chemical changes in bulk composition, or the generation of fault gouge) often accompanies fault rupture [*Kostrov and Das*, 1988; *Scholz*, 1990; *Beeler and Tullis*, 1997]. These changes to the fault properties may occur rapidly and are not reversible on short timescales.

[6] We pose the hypothesis that main shock-generated positive $\Delta$CFS($t$) moves an aftershock fault closer to failure by modifying the aftershock fault or its environs. Unlike some previous studies that investigate dynamic triggering of earthquakes coincident with the seismic waves passage [e.g., *Belardinelli et al.*, 1999; *Henry et al.*, 2000; *Voisin et al.*, 2000; *Power et al.*, 2001], we allow for delayed (days to months)

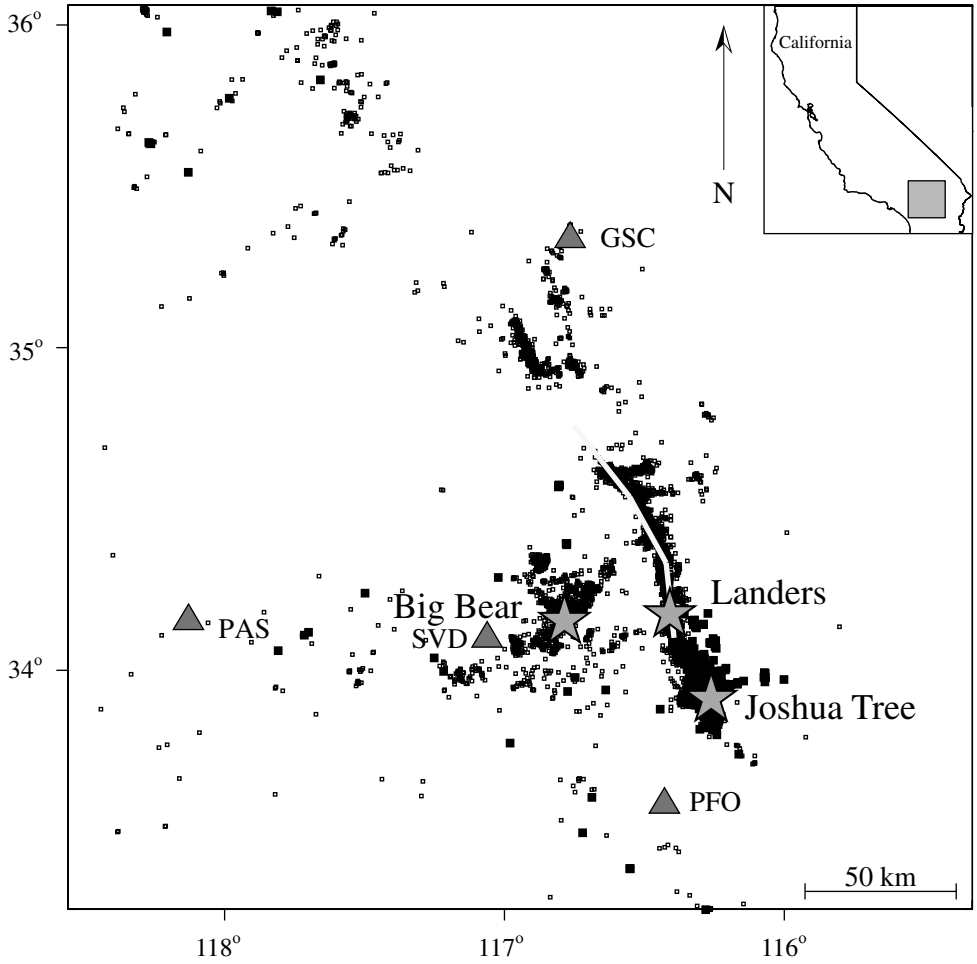


**Figure 2.** Map view of the southern California *M*6.1 Joshua tree (23 April 1992; 33.97°, −116.32°), *M*7.3 Landers (28 June 1992; 34.22°, −116.43°), and *M*6.2 Big Bear (28 June 1992; 34.21°,−116.83°) earthquakes (stars) and their aftershocks (squares). Three linear segments depict the Landers main shock fault planes. Broadband TERRAscope stations (triangles) used in this study are also labeled. The Landers and Joshua tree earthquakes were primarily right lateral on vertical fault planes, whereas the favored focal plane for the Big Bear earthquake indicates left-lateral slip [*Hauksson et al.*, 1993; *Cotton and Campillo*, 1995; *Jones and Hough*, 1995]. Figures 5, 6, 8, and 9 cover the same 300 km by 300 km study region. For more information see Tables 2 and 3.

failure. A dynamically weakened fault may then fail as tectonic loading continues or if the failure process is far enough along that failure is self-accelerating. In these cases, failure may occur long after the dynamic stresses have ceased but earlier than if the weakening had not occurred. The latter results in an increase in seismicity rate. Another possibility is that the dynamic stresses cause formation of new fractures that subsequently fail after some delay time; in this case the seismicity rate is increased due to "extra" earthquakes.

[7] If our hypothesis is correct, then seismicity rate increases should correlate with large positive (peak) values of $\Delta CFS(t)$. While we acknowledge that mechanisms of dynamic strengthening exist [e.g., *Richardson and Marone*, 1999] that could lead to seismicity rate decreases, we only test the simplest hypothesis with the fewest degrees of freedom for this first-of-a-kind study. Because the precise mechanism of dynamic weakening is unknown, we chose the peak $\Delta CFS(t)$ as a gross measure of the dynamic stress change because it always occurs in the dynamic interval. Because the dynamic stress changes oscillate about zero, our results would be basically the same if we chose some other measure of the dynamic stress change (e.g., peak-to-peak amplitude or the most negative peak). We suggest dynamic stress changes promote failure (rather than inhibit it), but our analysis cannot distinguish among weakening mechanisms. Future work may examine other aspects of the dynamic stress changes (e.g., duration of large oscillatory stress changes, dependence on frequency content) and their possible correlation with seismicity rate change.

[8] We test our hypothesis using data from and analysis of the 1992, *M*7.3, Landers earthquake in southern California. This earthquake was well recorded and has a relatively simple and well-constrained source mechanism, and appropriate seismicity data are readily available. Importantly, the Landers earthquake ruptured essentially unilaterally with strong directivity clearly affecting the radiated wave field. We thus expect the patterns of peak $\Delta CFS(t)$ and $\Delta CFS$ to differ, producing similar differences in their correlation with seismicity rate change patterns. Our analysis begins by constraining estimates of $\Delta CFS(t)$, from which we derive peak $\Delta CFS(t)$ and $\Delta CFS$. From catalog data we estimate seismicity rate changes associated with the Landers earthquake. We then compare mapped seismicity rate changes with mapped $\Delta CFS$ and peak $\Delta CFS(t)$ and assume that correlation implies causality. This assumption is not always valid, but it provides a reasonable starting point for testing our hypothesis. We evaluate this correla-

**Table 1.** Velocity Model Used in This Study[a]

| Layer Top, km | $V_p$, km/s | $V_s$, km/s | Density g/cm$^3$ | $Q_p$ | $Q_s$ |
|---|---|---|---|---|---|
| 0.0 | 3.80 | 1.98 | 2.30 | 100. | 30. |
| 1.5 | 5.50 | 3.15 | 2.60 | 600. | 300. |
| 4.0 | 6.20 | 3.52 | 2.70 | 600 | 300. |
| 26.0 | 6.80 | 3.83 | 2.87 | 600 | 300. |
| 32.0 | 8.00 | 4.64 | 3.50 | 600 | 300. |

[a] Velocity model is from *Wald and Heaton* [1994].

tion quantitatively as well as qualitatively. Our results show that peak $\Delta$CFS($t$) is quantitatively as viable a triggering agent as $\Delta$CFS.

## 2. $\Delta$CFS($t$)

### 2.1. Coulomb Failure Criteria

[9] On a fault of a given orientation, time-dependent Coulomb failure stress change is defined as

$$\Delta\mathrm{CFS}(t) = \Delta\tau(t) - \mu[\Delta\sigma_n(t) - \Delta P(t)], \quad (1)$$

where $\tau$ is shear stress (positive in the rake direction), $\sigma_n$ is the stress normal to the fault (positive in compression), $P$ is the pore pressure (positive in compression), and $\mu$ is the coefficient of friction [*Harris*, 1998]. We assume an isotropic homogeneous poroelastic material and approximate the pore pressure change by

$$\Delta P(t) = S\frac{1}{3}[\Delta\sigma_{11}(t) + \Delta\sigma_{22}(t) + \Delta\sigma_{33}(t)], \quad (2)$$

where $S$ is Skempton's coefficient. We assume $S = 0.85$ and $\mu = 0.6$ [*Byerlee*, 1978; *Harris*, 1998]. Variations in these parameters influence some regions more than others, but overall our results are insensitive to reasonable variations in them ($0.5 \leq S \leq 1.0$ and $0.2 \leq \mu \leq 0.8$). Equation (1) also applies to the static case when $\Delta$CFS($t$) becomes constant (i.e., for large $t$, $\Delta$CFS($t$) = $\Delta$CFS). The individual components $\Delta\tau(t)$, $\Delta\sigma_n(t)$, and $\Delta$P($t$) do not necessarily reach their maximum at the same time as $\Delta$CFS($t$). Thus conclusions based on $\Delta$CFS or peak $\Delta$CFS($t$) do not necessarily hold true for $\Delta\tau(t)$, $\Delta\sigma_n(t)$, and $\Delta$P($t$) [*Parsons et al.*, 1999].

[10] A commonly employed failure criterion invokes an absolute level of Coulomb stress that when exceeded causes instantaneous rupture. This is consistent with the simple interpretation that a positive or negative value of $\Delta$CFS($t$) brings a fault closer to or farther from failure, respectively. However, this simple interpretation does not explain the delay time observed between main shocks and their aftershocks. Nor does it explain how the time to failure could be modified by transient dynamic stress changes. Thus instead of an absolute stress threshold we consider the important criterion to be a failure stress change threshold. Stress changes (see equation (1)) that exceed the threshold may alter fault properties sufficiently either to advance the time to failure of "inevitable" earthquakes or to induce the formation of new instabilities [*Marone*, 2000]. These processes need not result in a failure time advancement that is simply proportional to the stress change magnitude. If this proportionality existed, all aftershocks would occur at roughly the same time, a scenario that is clearly not true as evident in the extended duration of aftershock sequences.

### 2.2. Observational Constraints on $\Delta$CFS($t$)

[11] We constrain input parameters (e.g., earth structure, fault locations, rupture velocity, slip model, source function, and duration) required for our calculations of $\Delta$CFS($t$) by forward modeling recorded displacement waveforms (doubly integrated from acceleration) from the 1992 Landers earthquake. We assume that if our model replicates surface displacements correctly, it also provides accurate estimates of the deformation field at depth. This provides observational constraints on stress change calculations that are not often utilized in similar studies. We use the same algorithms and input parameters to model displacement seismograms and $\Delta$CFS($t$), employing a discrete wave number reflectivity method in an elastic plane-layered medium [*Cotton and Coutant*, 1997; *Belardinelli et al.*, 1999]. $\Delta$CFS estimates are confirmed using a numerical three-dimensional dislocation program [*Gomberg and Ellis*, 1994].

[12] We model twice-integrated three-component broadband accelerograms of the Landers' main shock recorded at TERRAscope stations (Figure 2) [*Kanamori et al.*, 1991]. We band-pass filter these acceleration data from 0.077 to 0.5 Hz using a second-order Butterworth filter and then integrate them twice to obtain displacements. This passband eliminates high frequencies that require a more detailed velocity structure to model and eliminates low-frequency noise that integration would amplify [*Cohee and Beroza*, 1994; *Wald and Heaton*, 1994; *Cotton and Campillo*, 1995]. Numerous researchers have modeled these waveforms [*Campillo and Archuleta*, 1993; *Cohee and Beroza*, 1994; *Dreger*, 1994; *Wald and Heaton*, 1994; *Cotton and Campillo*, 1995; *Gomberg*, 1996], and although the final parameters that we use differ from theirs in detail, because of the nonlinearity of the problem and sensitivity to different computational algorithms, our parameters are within the range of published values. We qualitatively judge the goodness of fit between observed and synthetic waveforms, giving priority to larger-amplitude waveforms, requiring the polarity of first motions to match, and emphasizing agreement in the initial several cycles. The synthetics must correctly reproduce the relative maximum amplitudes of the three components at each station, and the durations and frequency contents must be similar. Consequently, we give preference to modeling the horizontal data, which dominate this passband. Finally, the mod-

**Table 2.** Fault Model Parameters for the 1992 $M$7.3 Landers, the 1992 $M$6.1 Joshua Tree, and the Big Bear Earthquakes[a]

| | Johnson Valley | Homestead Valley | Camprock | Joshua Tree | Big Bear |
|---|---|---|---|---|---|
| Strike | 354° | 331° | 332° | 350° | 55° |
| Dip | 90° | 90° | 90° | 90° | 90° |
| Rake | 180° | 180° | 180° | 180° | 0° |
| Number of subfaults along strike | 4 | 4 | 4 | 5 | 5 |
| Number of subfaults along dip | 3 | 3 | 3 | 4 | 4 |
| Length, km | 25 | 25 | 30 | 12 | 15 |
| Width, km | 17 | 17 | 17 | 15 | 13 |
| Average slip, m | 1.03 | 1.78 | 0.755 | 0.5 | 0.83 |
| Percent of total Landers' moment | 39 | 35 | 26 | – | – |

[a] Earthquake data are from *Hauksson et al.* [1993], *Cotton and Campillo* [1995], and *Jones and Hough* [1995] for Landers, *Hauksson et al.* [1993] for Joshua Tree, and *Jones and Hough* [1995] for Big Bear.

**Table 3.** Slip Model of the Landers Main Shock Used for Synthetic Calculations[a]

| Camprock Fault | | | |
|---|---|---|---|
| Northwest | | Southeast | |
| Camp 1 (60–52.5 km) | Camp 2 (52.5–45 km) | Camp 3 (45–37.5 km) | Camp 4 (37.5–30 km) |
| – | 6.9 | 4.5 | 3.0 |
| 6.0 | – | 6.0 | – |
| – | 6.0 | 6.3 | 7.5 |
| **Homestead Valley Fault** | | | |
| Northwest | | Southeast | |
| Home 1 (30–25 km) | Home 2 (25–20 km) | Home 3 (20–15 km) | Home 4 (15–10 km) |
| – | 7.35 | 6.99 | 7.95 |
| – | 9.6 | 16.5 | – |
| 7.32 | 8.625 | 12.0 | 3.6 |
| **Johnson Valley Fault** | | | |
| Northwest | | Southeast | |
| JV 1 (10–5 km) | JV 2 (5–0 km) | JV 3 (0 to −5 km) | JV 4 (−5 to −10 km) |
| 5.1 | – | – | – |
| 6.0 | 6.0 | – | – |
| 9.6 | 12.6 | – | 1.47 |

[a] Values indicate right-lateral displacement motion in meters. Numbers in parentheses refer to along-fault distance from the main shock hypocenter. See Table 2 for additional information.

eled seismic moment and slip distribution must agree with published results.

[13] We use the velocity model of *Wald and Heaton* [1994] (Table 1) because it contains a thin low-velocity layer at the surface, which is needed to reproduce the surface waves at station GSC. To model the rupture, we distribute 23-point sources over three nonoverlapping planar faults representing the Johnson Valley, Homestead Valley, and Camprock faults (Tables 2 and 3). This number of point sources is substantially fewer than used in other models (e.g., *Cohee and Beroza* [1994], *Belardinelli et al.* [1999], and *Cotton and Campillo* [1995] used over 200, 500, and 3000 sources, respectively). This is possible because we use a simple directivity filter based on a Haskell model of unilateral rupture [*Aki and Richards*, 1980; *Gomberg*, 1996], and we stagger the rupture time of each point source. We do not model the foreshock that occurred 3 s before the main energy release [*Abercrombie and Mori*, 1994]. Our source function is a modified step function with finite risetime. Each point source is assigned an onset time and a risetime (average 2.54 ± 1.78 s). Onset times generate rupture velocities ranging between 2.5 and 3.0 km/s, and slip must be right-lateral. The seismic moment of our model, $1.1 \times 10^{20}$ N m, is high, yet within the published bounds (see summary by *Cohee and Beroza* [1994]). Our final synthetic waveforms are shown in Figure 3.

[14] The main shock-induced $\Delta$CFS($t$) and $\Delta$CFS calculations require selection of a fault plane and slip orientation, on which stresses are resolved, at observation points throughout our study region. To help select appropriate values, we use histograms of focal mechanism parameters. Of the 6599 cataloged Landers aftershocks, 43% have focal mechanism parameters derived from first motions (J. G. Armbruster and L. Seeber, personal communication, 1998)(Southern California Seismic Network (SCSN)); 445 of these belong to our declustered data set (see section 3). These focal mechanism parameters (both the entire and declustered sets) show no systematic dependence on location. Histogram peaks indicate primarily strike-slip motion on steeply dipping faults striking at ~330° (Figure 4). This mechanism is consistent with other larger-magnitude events in the region [*Jones and Helmberger*, 1998], and the strike is consistent with mapped faults in the area [*Dokka and Travis*, 1990; *Unruh et al.*, 1996]. We address the influence of variations in these parameters in section 4.1.

### 2.3. General Characteristics of $\Delta$CFS($t$)

[15] We compute $\Delta$CFS and peak $\Delta$CFS($t$) maps at the surface as well as depths of 2, 4.5, and 11 km, consistent with the 1992 Landers' aftershock depth distribution [*Hauksson et al.*, 1993; *Jones and Helmberger*, 1998]. These maps are derived from calculations of $\Delta$CFS($t$) at 271 points on right-lateral, vertical faults striking at 330°. We distribute these 271 points in concentric annuli about the main shock fault planes, such that more distant annuli have a sparser distribution of points. We measure $\Delta$CFS and peak $\Delta$CFS($t$) and linearly interpolate these results into square cells (6 km on a side) distributed uniformly throughout our study area. The mapped patterns of both $\Delta$CFS and peak $\Delta$CFS($t$) do not change significantly with depth, although the absolute amplitudes can be influenced by material properties. For example, $\Delta$CFS is generally smaller within the low-velocity surface layer than in a higher velocity layer at 4.5 km depth. This is not a consequence of the stress free surface boundary conditions because a simpler velocity model, without the low-velocity zone, yields a continual decrease in modeled $\Delta$CFS with depth. Similar results hold for peak $\Delta$CFS($t$).

[16] No single stress change component ($\Delta\tau(t)$, $\Delta\sigma_n(t)$, or $\Delta P(t)$, and the static equivalents) consistently dominates $\Delta$CFS($t$) or $\Delta$CFS. Off-fault lobes of large peak $\Delta$CFS($t$) in the southeast are primarily due to contributions from $\Delta\tau(t)$ and $\Delta P(t)$, whereas $\Delta\tau(t)$ and $\Delta\sigma_n(t)$ dominate large amplitude lobes in the northwest (Figure 5a). The same is true for $\Delta$CFS (Figure 5b). Qualitatively, the individual components correlate with the seismicity rate change but not as well as peak $\Delta$CFS($t$) does. For example, maps of peak $\Delta\tau(t)$ and peak $\Delta\sigma_n(t)$ exhibit asymmetries similar to peak $\Delta$CFS($t$), although rotated more clockwise. More rigorous tests, beyond the scope of this study, are required to determine if the components correlate with seismicity rate change

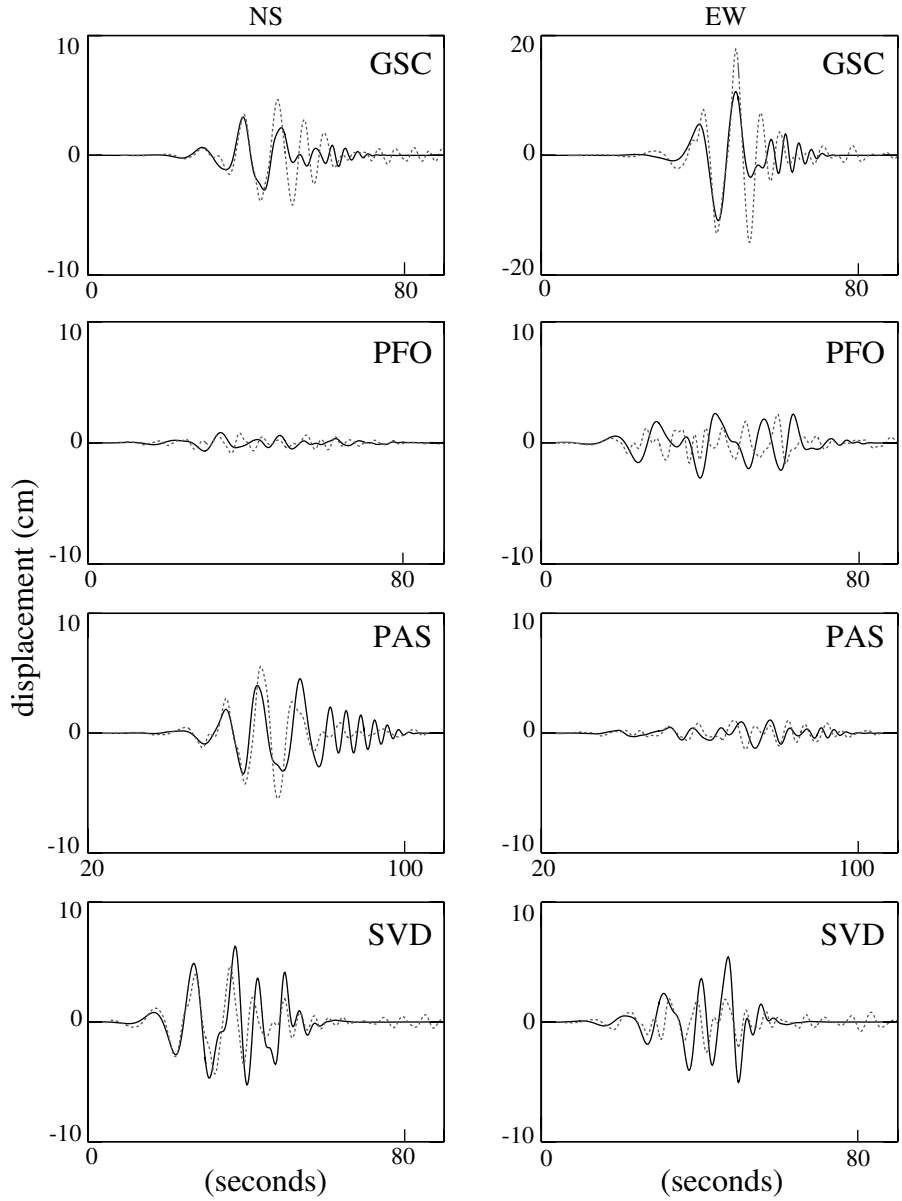


**Figure 3.** A comparison of the synthetic displacement seismograms (solid) and data (dashed) recorded at broadband TERRAscope stations (station codes are listed).

as well as or better than ΔCFS (e.g., as from *Parsons et al.* [1999], *Astiz et al.* [2000], and *Parsons and Dreger* [2000]) or peak ΔCFS($t$).

## 3. Estimating Seismicity Rate Change

[17] We use events from the SCSN catalog to constrain the seismicity rate change. A background seismicity rate was established using data (3498 events) from 1 July 1984 through 22 April 1992, since this time period was free of $M > 6$ events, significant network changes, and recording gaps. Data after the Landers main shock (6599 events) through 31 March 1993 are used to establish a post-main shock seismicity rate. To assure a uniform level of catalog completeness, our data set includes only $M \geq 2.2$ events [*Wald et al.*, 1998]. The temporal constancy of this limit was determined by selecting, for each year of data, the minimum magnitude above which the $b$ value was constant [*Toda et al.*, 1998]. Our data set includes only the highest quality events ("A" quality as defined in the SCSN catalog).

[18] The Landers aftershock sequence overlaps with aftershocks of the $M$6.1 Joshua Tree and $M$6.2 Big Bear earthquakes. Contributions from the Joshua Tree sequence to seismicity rates after the Landers main shock are negligible. In the 67 days between the Joshua Tree and Landers main shocks the seismicity fell from ~300 to ~3 $d^{-1}$, compared to an initial post-Landers' rate of ~360 $d^{-1}$. Both aftershock sequences decay according to Omori's law with typical decay constants of $0.72 \leq P \leq 1.2$ [*Hauksson et al.*, 1993]. We address the potential impact of the Big Bear earthquake on our results in section 4.1.

[19] We assume that all earthquakes are independent except for the dependence of the aftershocks on the Landers main shock. In an attempt to eliminate events that do not satisfy this assumption, we decluster our data set using a single-link cluster (SLC) analysis [*Frohlich and Davis*, 1990; *Davis and Frohlich*, 1991]. On the

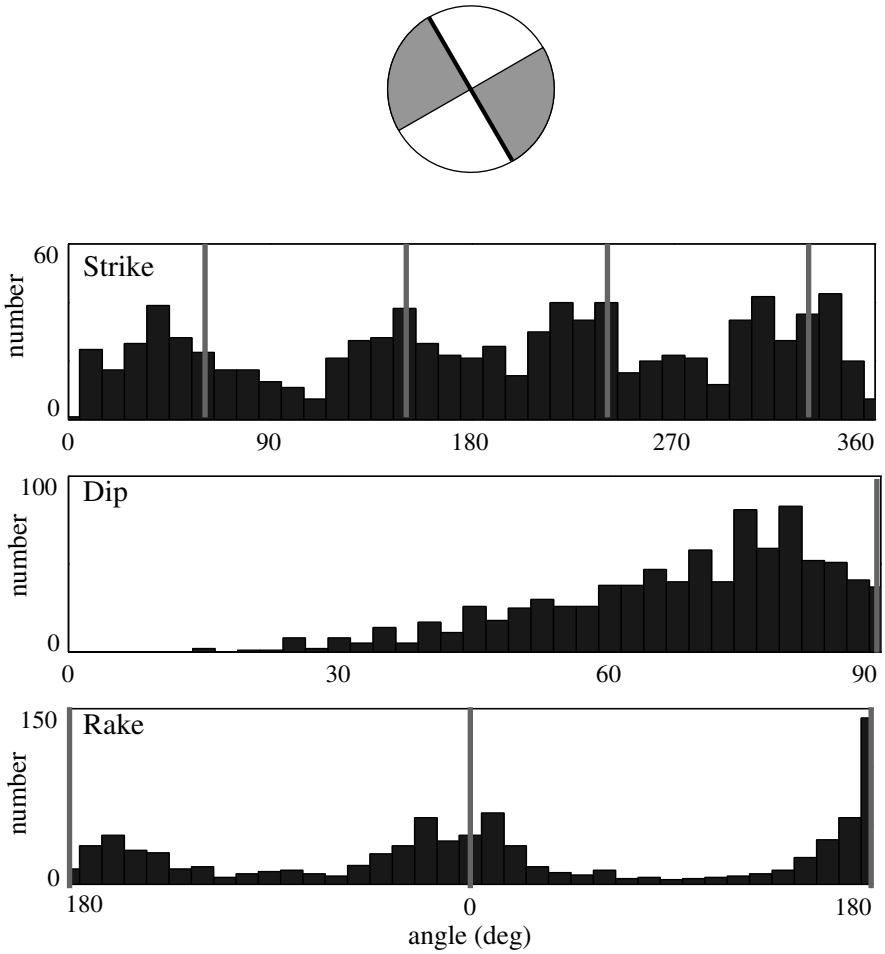


**Figure 4.** Histograms of both nodal planes from 445 available focal mechanisms in our declustered data set. Similar results are obtained using available mechanisms from the nondeclustered data set. Also shown is the focal mechanism corresponding to the approximate histogram peak values, where the bold line emphasizes the nodal plane striking at 330° used in our $\Delta$CFS($t$) calculations. Because variations in dip do not significantly affect our results, for simplicity, we assume a vertical fault plane.

basis of a defined tolerance within which two events are deemed related, the SLC($d,T$) metric identifies linked pairs of events. Clusters are formed by joining linked pairs that are also within this tolerance. For any pair of events the metric

$$\mathrm{SLC}(d,T) = \sqrt{d^2 + C^2T^2} \tag{3}$$

is defined where $d$ is the hypocentral separation between events, $T$ is the time difference in days, and $C$ is a constant that relates time to distance, usually set equal to 1. We use a tolerance value of 5, which corresponds to two "connected" earthquakes at the same location 5 days apart, or two simultaneous earthquakes within 5 km. The results are essentially identical when the tolerance is varied by ±2. The average event magnitude in our data set is $\sim M2.6$, which implies an average fault length $\ll$5 km. Thus this declustering criterion is conservative (40% of the events are removed) and should insure that our independence assumption is appropriate. Visually, the declustered map of seismicity is similar to the clustered catalog (compare Figures 2 and 6a).

[20] Estimation of seismicity rate changes requires subjective judgment about what changes are significant. To assist in this judgment we compute a $\beta$ statistic in each cell of a grid covering our study area [*Matthews and Reasenberg*, 1988; *Reasenberg and Simpson*, 1992]. The $\beta$ statistic measures the difference between the observed number of post-main shock earthquakes in a cell and the number expected based on an average seismicity rate determined using the pre-main shock events. This value is scaled by the seismicity rate's standard deviation so that small rate changes where the rate is relatively stationary may be ascribed as much significance as large rate changes where the rate fluctuates more. The $\beta$ statistic is defined by

$$\beta(n_a, n_b, t_a, t_b,) = \frac{n_a - E(n_a)}{\mathrm{Var}(n_a)} = \frac{n_a - (n_b t_a/t_b)}{n_b t_a/(t_a + t_b)}, \tag{4}$$

where $n$ is the number of earthquakes, $t$ is duration, and the subscripts $a$ and $b$ indicate the periods after and before the main shock, respectively. $E(n_a)$, is the expected value of $n_a$, and Var($n_a$), the variance of $n_a$, both values are based on the background period of seismicity [*Matthews and Reasenberg*, 1988; *Reasenberg and Simpson*, 1992]. When no earthquakes occur in the before period, $n_b = 0$ and (4) becomes singular. However, the observation of $n_b = 0$ does not imply that the rate is zero but that the rate is $<1/t_b$. Noting that when $n_b = 0$, $0.0 \leq E(n_b) < 0.5$, so that the unbiased estimate of $E(n_b) = 0.25$ and the best estimate of the rate is not zero but $0.25/t_b$. Thus when no earthquakes occur in the before period, we assume that $n_b = 0.25$.

[21] We regard a rate change as significant when $|\beta| \geq 1$ (Figure 6b) which, if seismicity represented a stationary Poisson

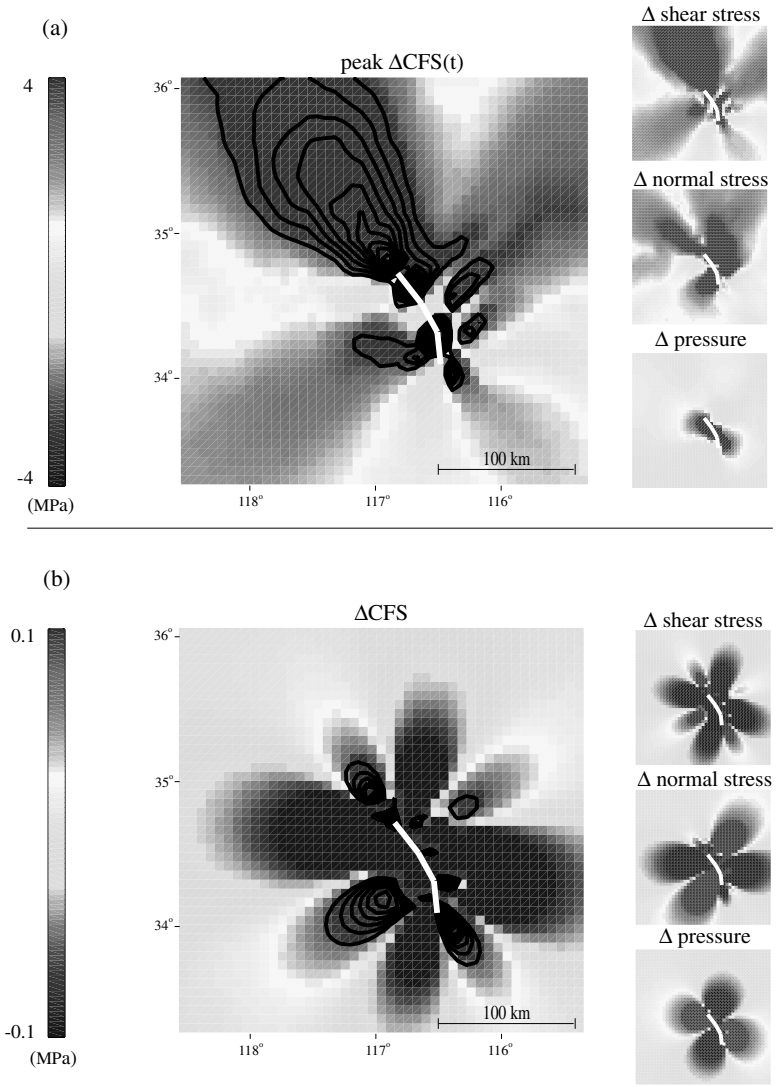


**Figure 5.** (a) Map at 4.5 km depth of peak $\Delta$CFS($t$) with contours indicating levels of peak $\Delta$CFS($t$) $\geq$ 4 MPa with equal intervals of 1.5 MPa. Peak $\Delta$CFS($t$) values are, by definition, always positive. Also shown are maps of the individual components that compose the final peak $\Delta$CFS($t$) map. (b) As in Figure 5a but for a map of $\Delta$CFS with contours indicating levels of $\Delta$CFS($t$) $\geq$ 0.1 MPa with equal intervals of 0.05 MPa. See color version of this figure at back of this issue.

process, would correspond to a rate change equal to one standard deviation from the pre-main shock mean. While this corresponds to a significance level of only 65%, this choice compensates for the gridding, as discussed below, which makes the $\beta$ estimates conservative.

## 4. Correlation Analyses

[22] We apply statistical measures of correlation between stress change and seismicity rate change maps using three methods: a ternary map comparison, a two-dimensional cross-correlation statistic, and a null hypothesis test using an eightfold table [*Sachs*, 1984]. The first two methods constrain the triggering amplitudes or "thresholds" at or above which we expect a related seismicity rate change. The cross-correlation statistic takes into account the mapped stress gradients whereas the simpler ternary-map does not. Our final test, using an eightfold table, more generally examines the validity of introducing yet another earthquake-triggering model.

[23] Our first quantitative test compares rate change and stress change ternary maps, which are composed of grid cells with values $-1$, 0, 1. We create a ternary seismicity rate change map by assigning 0 to grid cells with $|\beta| < 1.0$, and 1 or $-1$ to grid cells with $\beta \geq 1.0$ and $\beta \leq -1.0$, respectively (see Figure 6b). We apply a similar procedure to the $\Delta$CFS and peak $\Delta$CFS($t$) maps calculated at a depth of 4.5 km, assigning a 0 where the stress change is less than a chosen stress change threshold, a 1 if it is above the threshold, or a $-1$ (applicable for only $\Delta$CFS) if it is less than the negative of the threshold. To compare rate and stress change maps, we count the number of grid cells that have the same value (1 and 1, $-1$ and $-1$, 0 and 0). Also, we allow for the possibility that a rate decrease is not detected because our pre-Landers study period is too short, by assuming agreement when $\Delta$CFS is negative and the rate change in a cell is zero due to lack of seismicity.

[24] To assess the significance of our results, we compare our correlation count with that expected for a random process. The latter equals the mean of a distribution of counts obtained for 500 repeated tests using a bootstrap resampling of our seismicity rate

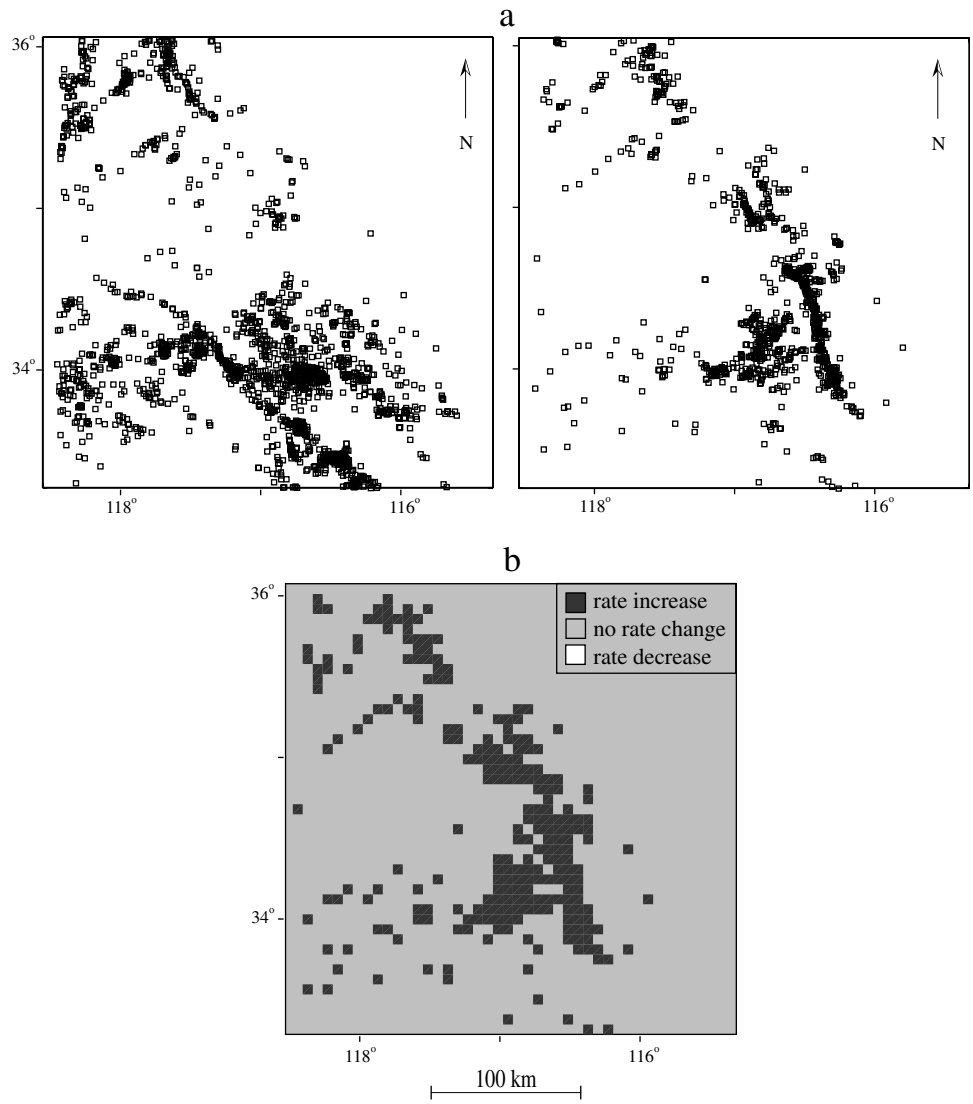


**Figure 6.** (a) Maps (left) of declustered background seismicity from 1 July 1984 to 23 April 1984 and (right) of declustered post Landers seismicity from 28 June 1992 to 31 March 1993. In the preseismicity map, lineation of events in the southwest quadrant of the study area outlines the San Andreas fault. (b) Ternary map of the seismicity rate change derived using the $\beta$ statistic. Only $\beta$ values that exceed one standard deviation (i.e., $|\beta| \geq 1$) are considered significant. The asymmetry observed in this rate change map mimics that computed with an independent analysis by *Wyss and Wiemer* [2000].

change maps. We deem the actual count significant if it lies outside the random distribution's mean by many standard deviations [*Sachs*, 1984; *Press et al.*, 1986] (Figure 7a). We assume a significant count implies a causal relationship between the seismicity rate change and stress changes ($\Delta$CFS or peak $\Delta$CFS($t$)) at or greater than the chosen threshold value. To determine the optimal triggering threshold, we repeat the ternary map randomization comparisons using various threshold values; the optimum threshold for triggering aftershocks yields the largest difference between the true value and random mean. This analysis shows that significant correlations exist for triggering thresholds of 0.001–0.5 MPa for $\Delta$CFS and >0.5 MPa for peak $\Delta$CFS($t$) (Figure 7b). The optimal triggering thresholds are 0.1 MPa for $\Delta$CFS and 4.0 MPa for peak $\Delta$CFS($t$).

[25] We also further assess the spatial similarity of stress and seismicity rate changes using a two-dimensional cross-correlation coefficient, which allows us to investigate the correlation of gradient changes. We compute the cross correlation after imposing a specific limit on the maximum stress change value in any cell. In this way, small maxima test for correlation with small gradients, and larger maxima test for correlation with larger gradients. As in the ternary map analysis, we search for ranges and optimum triggering thresholds using the same bootstrap procedure. Application of this approach shows that the seismicity rate change correlates significantly with peak $\Delta$CFS($t$) for all threshold values above 0.1 MPa and with $\Delta$CFS for thresholds of 0.0005–0.5 MPa. The $\Delta$CFS lower bound, 0.0005 MPa, is surprisingly small. This results from the stability of the four-lobe $\Delta$CFS pattern that simply expands as the stress change threshold decreases and which mimics, to some degree, the seismicity rate change pattern. The potential for a positive correlation also may be enhanced by the fact that we do not consider the magnitude of the seismicity rate change. This result may lend support to the proposal of *Ziv and Rubin* [2000] that the stress triggering threshold has no lower bound, but more work is required to evaluate its significance. In agreement with the ternary map comparison results the optimum

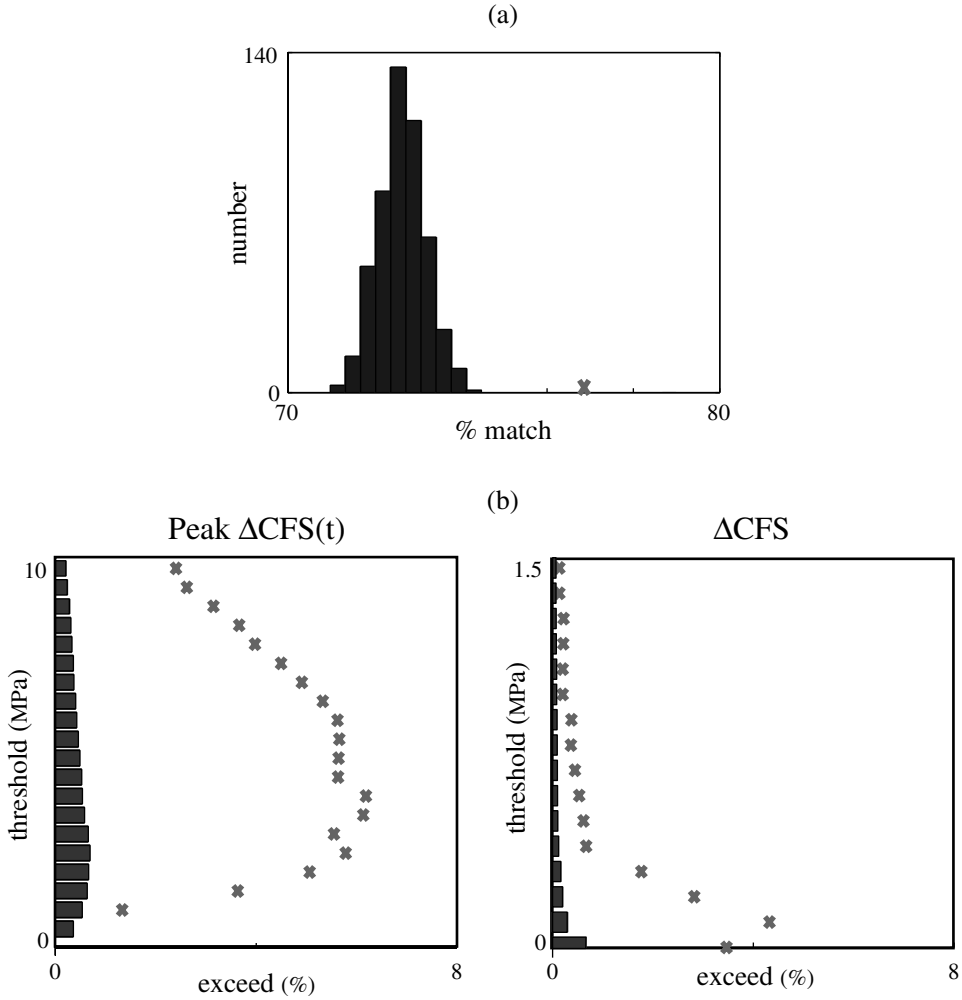


**Figure 7.** (a) Example histogram of 500 randomization correlation results. Correlations using ternary maps of randomly reordered rate change maps and peak ΔCFS($t$) are computed for a threshold value of 4 MPa. The true value (cross) lies outside of the random distribution (bars) by 6 standard deviations. These histograms are computed for a range of threshold values. (b) Similar results for different threshold levels for (left) peak ΔCFS($t$) and (right) ΔCFS. The $x$ axis measures the percentage above the random mean, the bars indicate the standard deviation, and the crosses are the true correlation values. More threshold values are investigated for the peak ΔCFS($t$) study than the ΔCFS study (note different $y$ axis scales) due to their larger range of attainable values.

triggering thresholds are 0.1 and 4.0 MPa for ΔCFS and peak ΔCFS($t$), respectively.

[26] Both the ternary map and cross-correlation analysis results suggest that stress changes correlate with seismicity rate changes by no more than 10% better than random. These results are conservative estimates for several reasons. First, our relatively short observation period makes it difficult to accurately capture seismicity rate changes, especially a decrease, for cells where the preevent seismicity rate is very low. More importantly, the rate change map depends highly on the grid cell size because we estimate rate change in an area based on point data (i.e., assuming each earthquake occurs at a point). We chose a 6 km by 6 km cell size to capture accurately the fluctuation in rate and stress changes close to the main shock fault, while also being consistent with our declustering parameters. The relatively smooth variation of ΔCFS and peak ΔCFS($t$) makes their maps less sensitive to cell size variations. While it is obvious visually that the correlation could be improved by increasing the cell size or by applying a smoothing operator, it is not clear how to do this objectively. Nonetheless, because our results are many standard deviations outside of the random distribution, we have demonstrated that both ΔCFS and peak ΔCFS($t$) correlate with seismicity rate change at a statistically significant level.

[27] It is clear visually that a smoother seismicity rate change map would improve the correlation for the peak ΔCFS($t$) map more than for the ΔCFS map, particularly in the northwest quadrant of our study area. Figure 8 superimposes contours of ΔCFS and peak ΔCFS($t$) at or above their optimal threshold on seismicity rate change maps. The most striking correlation is the asymmetry apparent in both the seismicity rate change and peak ΔCFS($t$) maps. The mapped peak ΔCFS($t$) asymmetry arises from directed northward rupture propagation that has no affect on ΔCFS, which consequently is more symmetric. Unfortunately, the better correlation for peak ΔCFS($t$) than for ΔCFS cannot be used to conclude that dynamic stress changes are more effective triggers than static stress changes. The better correlation may simply be a consequence of the greater contribution of dynamic stress changes to the total stress change as the distance increases.

[28] Finally, we examine the null hypothesis that the peak ΔCFS($t$) model does not correlate with seismicity rate change better than the ΔCFS model. To do this, our ternary map comparison results are used to define an eightfold table, and we

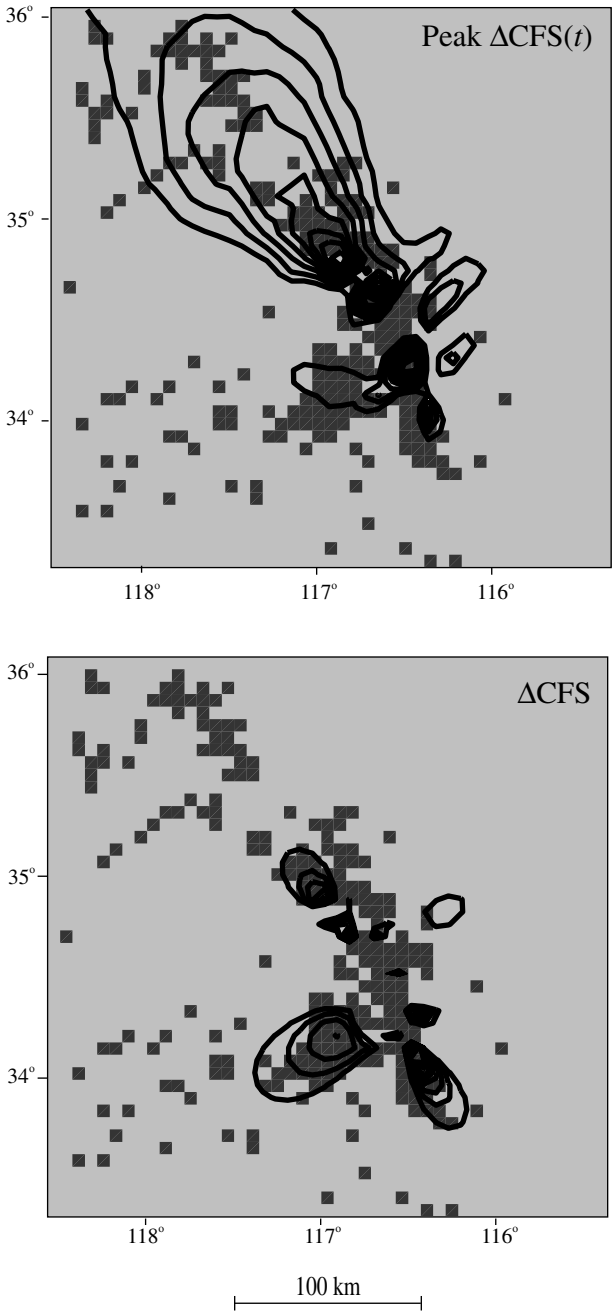


**Figure 8.** Contours of (top) peak $\Delta CFS(t) \geq 4$ MPa and (bottom) $\Delta CFS \geq 0.1$ MPa superimposed on rate change ternary maps. Ternary map shading indicate significant rate increases (black), decreases (white), and regions of no change (gray).

determine how much the table values deviate from the expected values if the results were model independent [*Sachs*, 1984]. Our results show we can reject the null hypothesis at the 99% level and infer that the peak $\Delta CFS(t)$ model correlates with seismicity rate change at least as well as the $\Delta CFS$ model.

### 4.1. Sensitivity Tests

[29] Our results are insensitive to reasonable variations (i.e., those found in the literature) of the friction or Skempton's coefficients, material properties, declustering parameters, and the $\beta$ statistic significance level. We attempt to test the sensitivity of our results due to errors in assumed failure plane orientation and slip direction required for the calculations of $\Delta CFS$ and peak $\Delta CFS(t)$. Unlike many studies that investigate optimally oriented failure planes [*Stein et al.*, 1992; *King et al.*, 1994; *Gross and Kisslinger*, 1997; *Toda et al.*, 1998], we assume that all observation planes have the same orientation (strike of 330°; dip of 90°) and slip direction (right lateral). For locations away from the main

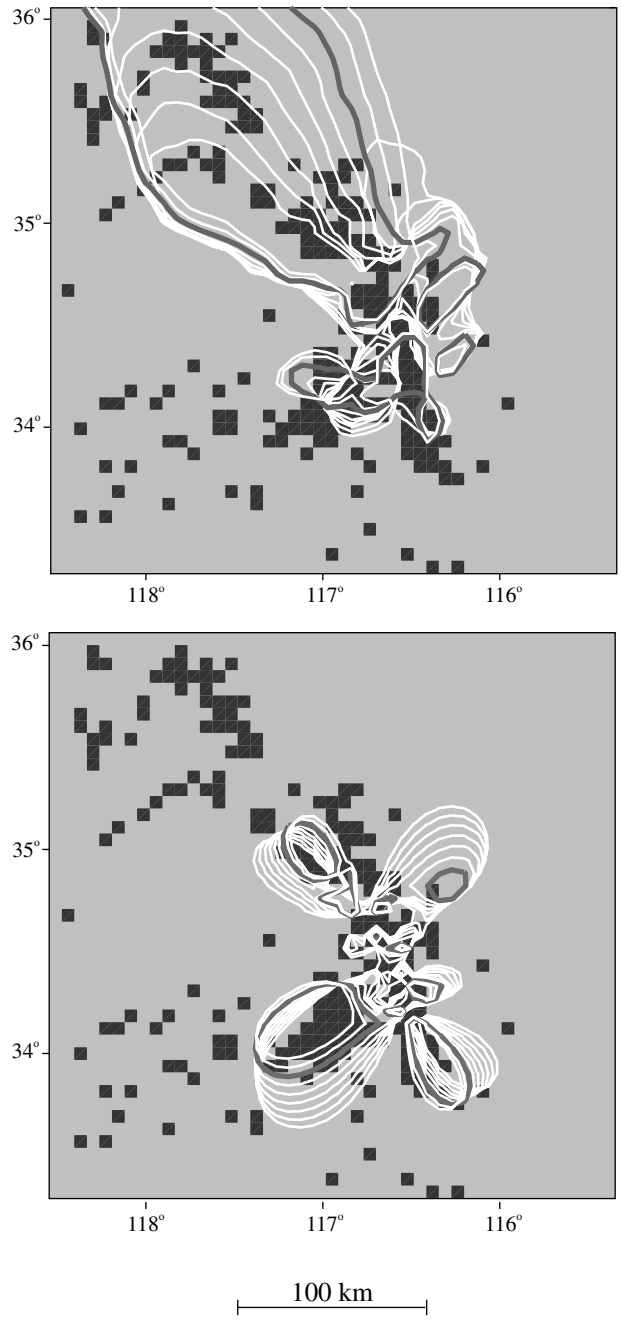


**Figure 9.** Mapped contours outlining (top) peak $\Delta CFS(t) \geq 4$ MPa and (bottom) $\Delta CFS \geq 0.1$ MPa for vertical right-lateral observation plane's with strikes ranging between 300° and 340°, as suggested by aftershock focal mechanisms (see Figure 4). Significant changes take place at regions away from the main shock fault. The bold contour indicates the preferred fault orientation used in this study. Contours are overlaid on the ternary seismicity rate change map described in Figure 6b. Ternary map shading indicates significant rate increases (black), decreases (white), and regions of no change (gray).

shock fault this orientation is nearly optimally oriented given the ~N7°E principal compressional background stress field orientation in the area [*Lisowski et al.*, 1991; *King et al.*, 1994]. For locations close to the fault (<10 km) the stress field, and consequently the optimally oriented failure planes, varies significantly [*Hardebeck et al.*, 1998]. However, this region encompasses <2% of our total study area. We find that our results are insensitive to observed variations in aftershock rake and dip parameters (see Figure 4), but variations in fault strike within the observed 40° range can cause the mapped ΔCFS and peak ΔCFS($t$) contours to rotate up to ~20° and the width of contoured stress lobes to change by a factor of 2 (Figure 9). Nonetheless, our final results appear relatively stable for such rotations.

[30] We do not explicitly incorporate in our analyses the stress changes associated with the $M$6.2 Big Bear earthquake, which occurred ~3 hours after and within 40 km of the Landers main shock [*Hauksson et al.*, 1993]. We did qualitatively compare ΔCFS and peak ΔCFS($t$) maps computed with and without stress changes from both the $M$6.1 Joshua Tree and $M$6.2 Big Bear earthquakes and found notable differences only in the immediate vicinity of these events. Some Big Bear aftershocks undoubtedly remain in our declustered catalog, and we do not rigorously assess their potential contribution because both Joshua Tree and Big Bear aftershocks affect only the southern portion of our study area. Our primary conclusions stem from the strong correlation between the asymmetries in seismicity rate and peak ΔCFS($t$) in the north, so a more rigorous accounting of the Big Bear and Joshua Tree earthquakes should not alter them.

## 5. Discussion

[31] Quantitative and qualitative assessments of the correlations between stress changes and seismicity rate changes indicate peak ΔCFS($t$) is, at minimum, as effective at triggering aftershocks as ΔCFS. We base this conclusion on the observation that the spatial distribution of peak ΔCFS($t$) shares the same asymmetry as that in the seismicity rate change. The asymmetry in the peak ΔCFS($t$) map results from the propagating rupture and consequent directivity, required to model the Landers earthquake seismograms. Directivity has no affect on ΔCFS, which depends only on the final permanent, relatively symmetric fault displacement. Thus the ΔCFS map lacks the asymmetry evident in the peak ΔCFS($t$) map. Others have suggested that asymmetry in aftershock locations may be due to directivity but did not explicitly demonstrate the relationship [e.g., *Hauksson et al.*, 1993; *King et al.*, 1994; *Toda et al.*, 1998]. The results of our statistical tests do not adequately reflect the similarities between the asymmetries in the peak ΔCFS($t$) and seismicity rate change maps, primarily because of the discretization of the rate change estimates. However, as Figure 8 shows, the correlation between the seismicity rate change and peak ΔCFS($t$) is compelling and more striking than the correlation with ΔCFS. We caution that this better correlation may simply reflect the greater contribution of dynamic stress changes to the total stress change as the distance increases and thus does not imply that dynamic stress changes are more effective triggers than static stress changes. To infer that either dynamic or static stress changes were more effective triggers, one would have to observe differences in correlations for peak ΔCFS($t$) and ΔCFS that could not be attributed to other effects (e.g., a better correlation for peak ΔCFS($t$) relative to that for ΔCFS closer to the fault than farther away, or a lack of correlation for only peak ΔCFS($t$) or only ΔCFS). Certainly, factors we have not accounted for, such as the distribution of available faults, spatial variations in rheology, and background stress field variations, may contribute to or detract from the estimated correlations [*Gomberg*, 1996; *Gross and Kisslinger*, 1997; *Mori and Abercrombie*, 1997; *Astiz et al.*, 2000].

[32] Despite a lack of a definitive physical interpretation, the large peak ΔCFS($t$) amplitudes, relative to ΔCFS amplitudes and earthquake stress drops, provide compelling support for dynamic triggering. If stress changes can facilitate delayed failure by physically altering the fault or its environs, larger changes should be more effective triggers. A number of specific alteration mechanisms might be considered. For example, laboratory tests indicate that fault rupture may result from the influence of an oscillatory normal stress field [*Brune et al.*, 1993]. *Bodin et al.* [1998] also propose that extensional normal displacements are responsible for promoting failure and perhaps help to sustain fault rupture. Also, theoretical computations of stress changes induced by the Umbria-Marche earthquake sequence find normal stress changes best correlate with the progression of moderate magnitude events [*Cocco et al.*, 2000]. Oscillating shear stress changes may break asperities that otherwise hinder fault slip [*Beeler and Tullis*, 1997]. These concepts are analogous to the back-and-forth motion that is used to move a large rock that is partially imbedded in a host material. Several mechanisms rely on the presence of fault gouge, with and without fluids. Rapid normal stress variations have been shown to compact and consolidate fault gouge material, which if saturated might act to raise pore pressures and weaken the fault [*Marone and Scholz*, 1988; *Scholz*, 1990; *Mora and Place*, 1999; *Richardson and Marone*, 1999]. In the absence of fluids, acoustic fluidization has been proposed as a fault weakening mechanism (see summary by *Sornette and Sornette* [2000]).

## 6. Conclusions

[33] Our objective was to assess the spatial correlation between Coulomb stress changes (ΔCFS or peak ΔCFS($t$)) and seismicity rate changes following the Landers $M$7.3 earthquake. We suggest that sufficiently large stress changes alter the physical and/or chemical properties of a fault and/or its environs and move the fault closer to failure. This alteration need not result in immediate failure, as it simply enhances the potential and allows for delayed failure.

[34] We find that mapped patterns of ΔCFS and peak ΔCFS($t$) differ in significant ways. Peak ΔCFS($t$) amplitudes exceed ΔCFS amplitudes by an order of magnitude or more, and this relative difference exists for all depths studied, although the absolute values may vary as material properties change. Similar results hold for the individual components that compose ΔCFS($t$) and ΔCFS ($\Delta\tau(t)$, $\Delta\sigma_n(t)$, and $\Delta P(t)$ and the static equivalents), although qualitatively correlations with seismicity rate change favor ΔCFS or peak ΔCFS($t$) over any of their components. The most convincing positive correlation is the asymmetry found in both mapped peak ΔCFS($t$) and seismicity rate change, which is not present in ΔCFS maps. The asymmetry in peak ΔCFS($t$) results from rupture directivity, which is required to model waveforms of the 1992 Landers earthquake. These results are not sensitive to reasonable errors in model parameters.

[35] Quantitative statistical tests demonstrate the following: (1) Peak ΔCFS($t$), which occurs during the interval of dynamic deformations, correlates at least as well as ΔCFS with changes in seismicity rate. (2) Both ΔCFS and peak ΔCFS($t$) correlate with seismicity rate change better, by ~10%, than the correlation expected if rate changes were a consequence of a random process. Although this 10% correlation difference may not seem compelling, it is highly statistically significant. This is also a very conservative estimate because of the statistical analysis applied. (3) For model parameters at a depth of 4.5 km, viable Coulomb stress triggering amplitude thresholds (i.e., stress changes above which they correlate significantly with seismicity rate change) are 0.001–0.5 MPa for ΔCFS, and any value ≥0.5 MPa for peak ΔCFS($t$). The optimal triggering threshold values are 0.1 and 4.0 MPa for ΔCFS and peak ΔCFS($t$), respectively.

[36] A qualitative visual assessment of the correlation between mapped ΔCFS and peak ΔCFS($t$) with seismicity rate change is much more compelling than the statistical results. Although the

asymmetry in the seismicity rate change pattern is mimicked only in the peak $\Delta CFS(t)$ map, this relatively better correlation may simply reflect an increasing contribution of dynamic stress changes to the total with increasing distance. Nonetheless, we can conclude it is probable that large peak $\Delta CFS(t)$ amplitudes (an order of magnitude larger than $\Delta CFS$ and >10% of the stress drop) are as effective as $\Delta CFS$ in triggering aftershocks. Therefore the physical process of aftershock triggering should account for the time-dependent nature of the dynamic stress changes. Future work should test this hypothesis using main shock-aftershock sequences in other regions to determine if these results are a global phenomenon.

[37] **Acknowledgments.** We thank F. Cotton and O. Coutant for helping/supplying us with their computer code that was an essential part of this work. The thoughtful reviews by G. Anderson, R. Harris, S. Prejean, R. Simpson, and A. Ziv greatly improved this paper. We also thank S. Davis and P. Reasenberg for helping us with statistical tests. This work was partially supported by U.S. Geological Survey NEHRP grant 98HQGR1021, and partial support for D. Kilb was provided by the Palisades Fellowship. CERI contribution 427.

## References

Abercrombie, R., and J. Mori, Local observations of the onset of a large earthquake: 28 June 1992 Landers, California, *Bull. Seismol. Soc. Am.*, *84*, 725–734, 1994.

Aki, K., and P. G. Richards, *Quantitative Seismology*, W. H. Freeman, New York, 1980.

Anderson, G., and H. Johnson, A new statistical test for static stress triggering: Application to the 1987 Superstition Hills earthquake sequence, *J. Geophys. Res.*, *104*, 20,153–20,168, 1999.

Anderson, J. G., J. N. Brune, J. N. Louie, Y. H. Zeng, M. Savage, G. Yu, Q. B. Chen, and D. dePolo, Seismicity in the western Great Basin apparently triggered by the Landers, California, earthquake 28 June 1992, *Bull. Seismol. Soc. Am.*, *84*, 863–891, 1994.

Astiz, L., P. M. Shearer, and D. C. Agnew, Precise relocations and stress change calculations for the Upland earthquake sequence in southern California, *J. Geophys. Res.*, *105*, 2937–2953, 2000.

Beeler, N. M., and T. E. Tullis, The roles of time and displacement in velocity-dependent volumetric strain of fault zones, *J. Geophys. Res.*, *102*, 22,595–22,609, 1997.

Belardinelli, E. M., M. Cocco, O. Coutant, and F. Cotton, Redistribution of dynamic stress during coseismic ruptures: Evidence for fault interaction and earthquake triggering, *J. Geophys. Res.*, *104*, 14,925–14,945, 1999.

Bennett, R. A., R. E. Reilinger, W. Rodi, and Y. Li, Coseismic fault slip associated with the 1992 $M_w$ 6.1 Joshua Tree, California, earthquake: Implications for the Joshua Tree-Landers earthquake sequence, *J. Geophys. Res.*, *100*, 6443–6461, 1995.

Bodin, P., S. Brown, and D. Matheson, Laboratory observations of fault-normal vibrations during stick slip, *J. Geophys. Res.*, *103*, 29,931–29,944, 1998.

Brune, J. N., S. Brown, and P. Johnson, Rupture mechanism and interface separation in foam rubber models of earthquakes: A possible solution to the heat flow paradox and the paradox of large overthrusts, *Tectonophysics*, *218*, 59–67, 1993.

Byerlee, J. D., Friction of rock, *Pure Appl. Geophys.*, *116*, 615–626, 1978.

Campillo, M., and R. J. Archuleta, A rupture model for the 28 June 1992 Landers, California, earthquake, *Geophys. Res. Lett.*, *20*, 647–650, 1993.

Cocco, M., C. Nostro, and G. Ekström, Static stress changes and fault interaction during the 1997 Umbria-Marche earthquake sequence, *J. Seismol.*, *4*, 501–516, 2000.

Cohee, B. P., and G. C. Beroza, Slip distribution of the 1992 Landers earthquake and its implications for earthquake source mechanics, *Bull. Seismol. Soc. Am.*, *84*, 692–712, 1994.

Cotton, F., and M. Campillo, Stability of the rake during the 1992, Landers earthquake: An indication for a small stress release?, *Geophys. Res. Lett.*, *22*, 1921–1924, 1995.

Cotton, F., and O. Coutant, Dynamic stress variations due to shear faults in a plane-layered medium, *Geophys. J. Int.*, *128*, 676–688, 1997.

Das, S., and C. H. Scholz, Off-fault aftershock clusters caused by shear stress increase?, *Bull. Seismol. Soc. Am.*, *71*, 1669–1675, 1981.

Davis, S. D., and C. Frohlich, Single-link cluster analysis of earthquake aftershocks: decay laws and regional variations, *J. Geophys. Res.*, *96*, 6335–6350, 1991.

Dodge, D. A., G. C. Beroza, and W. L. Ellsworth, Foreshock sequence of the 1992 Landers, California, earthquake and its implications for earthquake nucleation, *J. Geophys. Res.*, *100*, 9865–9880, 1995.

Dokka, R. K., and C. J. Travis, Late Cenozoic strike-slip faulting in the Mojave Desert, California, *Tectonics*, *9*, 311–340, 1990.

Dreger, D. S., Investigation of the rupture process of the 28 June 1992 Landers earthquake utilizing TERRAscope, *Bull. Seismol. Soc. Am.*, *84*, 713–724, 1994.

Du, Y., and A. Aydin, Stress transfer during three sequential moderate earthquakes along the central Calaveras fault, California, *J. Geophys. Res.*, *98*, 9947–9962, 1993.

Frohlich, C., and S. D. Davis, Single-link cluster analysis as a method to evaluate spatial and temporal properties of earthquake catalogues, *Geophys. J. Int.*, *100*, 19–32, 1990.

Gomberg, J., Stress/strain changes and triggered seismicity following the $M_w$ 7.3 Landers, California, earthquake, *J. Geophys. Res.*, *101*, 751–764, 1996.

Gomberg, J., and P. Bodin, Triggering of the Little Skull Mountain, Nevada earthquake with dynamic strains, *Bull. Seismol. Soc. Am.*, *84*, 844–853, 1994.

Gomberg, J., and S. Davis, Stress/strain changes and triggered seismicity at The Geysers, California, *J. Geophys. Res.*, *101*, 733–749, 1996.

Gomberg, J. S., and M. A. Ellis, Topography and tectonics of the central New Madrid Seismic zone: Results of numerical experiments using a three-dimensional boundary element program, *J. Geophys. Res.*, *99*, 20,299–20,310, 1994.

Gomberg, J., M. L. Blanpied, and N. M. Beeler, Transient triggering of near and distant earthquakes, *Bull. Seismol. Soc. Am.*, *87*, 294–309, 1997.

Gross, S., and C. Kisslinger, Estimating tectonic stress rate and state with Landers aftershocks, *J. Geophys. Res.*, *102*, 7603–7612, 1997.

Hardebeck, J. L., J. J. Nazareth, and E. Hauksson, The static stress change triggering model: Constraints from two southern California aftershocks sequences, *J. Geophys. Res.*, *103*, 24,427–24,437, 1998.

Harris, R. A., Introduction to special section: Stress triggers, stress shadows, and implications for seismic hazard, *J. Geophys. Res.*, *103*, 24,347–24,358, 1998.

Harris, R. A., and R. W. Simpson, Changes in static stress on southern California faults after the 1992 Landers earthquake, *Nature*, *360*, 251–254, 1992.

Hauksson, E., L. M. Jones, K. Hutton, and D. Eberhart-Phillips, The 1992 Landers earthquake sequence: Seismological observations, *J. Geophys. Res.*, *98*, 19,835–19,858, 1993.

Henry, C., S. Das, and J. H. Woodhouse, The great March 25, 1998, Antarctic Plate earthquake: Moment tensor and rupture history, *J. Geophys. Res.*, *105*, 16,079–16,118, 2000.

Hill, D. P., et al., Seismicity remotely triggered by the magnitude 7.3 Landers, California, earthquake, *Science*, *260*, 1617–1623, 1993.

Hill, D. P., M. J. S. Johnston, J. O. Langbein, and R. Bilham, Response of Long Valley caldera to the $M_w$ = 7.3 Landers, California, earthquake, *J. Geophys. Res.*, *100*, 12,985–13,005, 1995.

Jones, L. E., and D. V. Helmberger, Earthquake source parameters and fault kinematics in the Eastern California Shear Zone, *Bull. Seismol. Soc. Am.*, *88*, 1337–1352, 1998.

Jones, L. E., and S. E. Hough, Analysis of broadband records from the 28 June 1992 Big Bear earthquake: Evidence of a multiple-event source, *Bull. Seismol. Soc. Am.*, *85*, 688–704, 1995.

Kanamori, H., E. Hauksson, and T. Heaton, TERRAscope and CUBE project at Caltech, *Eos Trans. AGU*, *72*, 564, 1991.

King, G. C. P., R. S. Stein, and J. Lin, Static stress changes and the triggering of earthquakes, *Bull. Seismol. Soc. Am.*, *84*, 935–953, 1994.

Kostrov, B. V., and S. Das, *Principles of Earthquake Source Mechanics*, Cambridge Univ. Press, New York, 1988.

Lisowski, M., J. C. Savage, and W. H. Prescott, The velocity field along the San Andreas fault in central and southern California, *J. Geophys. Res.*, *96*, 8369–8389, 1991.

Marone, C., Shaking faults loose, *Nature*, *408*, 533–535, 2000.

Marone, C., and C. Scholz, Frictional behavior and constitutive modeling of simulated fault gouge, *Geophys. Res. Lett.*, *15*, 621–624, 1988.

Matthews, M. V., and P. A. Reasenberg, Statistical methods for investigating quiescence and other temporal seismicity patterns, *Pure Appl. Geophys.*, *126*, 357–372, 1988.

Mora, P., and D. Place, The weakness of earthquake faults, *Geophys. Res. Lett.*, *26*, 123–126, 1999.

Mori, J., and R. E. Abercrombie, Depth dependence of earthquake frequency-magnitude distributions in California: Implications for rupture initiation, *J. Geophys. Res.*, *102*, 15,081–15,090, 1997.

Nostro, C., M. Cocco, and M. E. Belardinelli, Static stress changes in extensional regimes: an application to southern Apennines (Italy), *Bull. Seismol. Soc. Am.*, *87*, 234–248, 1997.

Parsons, T., and D. S. Dreger, Static-stress impact of the 1992 Landers earthquake sequence on nucleation and slip at the site of the 1999 $M$ = 7.1 Hector Mine earthquake, southern California, *Geophys. Res. Lett.*, *27*, 1949–1952, 2000.

Parsons, T., R. S. Stein, R. W. Simpson, and P. A. Reasenberg, Stress sensitivity of fault seismicity: A comparison between limited-offset oblique and major strike-slip faults, *J. Geophys. Res.*, *104*, 20,183–20,202, 1999.

Power, J. A., S. C. Moran, S. R. McNutt, S. D. Stihler, and J. J. Sanchez, Seismic response of the Katmai volcanoes to the 6 December 1999 magnitude 7.0 Karluk Lake earthquake, Alaska, *Bull. Seismol. Soc. Am.*, *91*, 57–63, 2001.

Press, W. H., B. P. Flannery, S. A. Teukolsky, and W. T. Vetterling, *Numerical Recipes: The Art of Scientific Computing*, Cambridge Univ. Press, New York, 1986.

Reasenberg, P. A., and R. W. Simpson, Response of regional seismicity to the static stress change produced by the Loma Prieta earthquake, *Science*, *255*, 1687–1690, 1992.

Richardson, E., and C. Marone, Effects of normal stress vibrations on frictional healing, *J. Geophys. Res.*, *104*, 28,857–28,878, 1999.

Rybicki, K., T. Kato, and K. Kasahara, Mechanical interaction between neighboring active faults—Static and dynamic stress field induced by faulting, *Bull. Earthquake Res. Inst. Univ. Tokyo*, *60*, 1–21, 1985.

Sachs, L., *Applied Statistics: A Handbook of Techniques*, Springer-Verlag, New York, 1984.

Scholz, C. H., *The Mechanics of Earthquakes and Faulting*, Cambridge Univ. Press., New York, 1990.

Sornette, D., and A. Sornette, Acoustic fluidization for earthquakes?, *Bull. Seismol. Soc. Am.*, *90*, 781–785, 2000.

Stein, R. S., The role of stress transfer in earthquake occurrence, *Nature*, *402*, 605–609, 1999.

Stein, R. S., and M. Lisowski, The 1979 Homestead Valley earthquake sequence, California: Control of aftershocks and postseismic deformation, *J. Geophys. Res.*, *88*, 6477–6490, 1983.

Stein, R. S., G. C. P. King, and J. Lin, Change in failure stress on the southern San Andreas Fault system caused by the 1992 magnitude = 7.4 Landers earthquake, *Science*, *258*, 1328–1332, 1992.

Toda, S., R. S. Stein, P. A. Reasenberg, J. H. Dieterich, and A. Yoshida, Stress transferred by the 1995 $M_w$ = 6.9 Kobe, Japan, shock: Effect on aftershocks and future earthquake probabilities, *J. Geophys. Res.*, *103*, 24,543–24,565, 1998.

Unruh, J. R., R. J. Twiss, and E. Hauksson, Seismogenic deformation field in the Mojave block and implications for tectonics of the eastern California shear zone, *J. Geophys. Res.*, *101*, 8335–8361, 1996.

Voisin, C., M. Campillo, I. R. Ionescu, F. Cotton, and O. Scotti, Dynamic versus static stress triggering and friction parameters: Inferences from the November 23, 1980, Irpinia earthquake, *J. Geophys. Res.*, *105*, 21,647–21,659, 2000.

Wald, D. J., and T. H. Heaton, Spatial and temporal distribution of slip for the 1992 Landers, California, earthquake, *Bull. Seismol. Soc. Am.*, *84*, 668–691, 1994.

Wald, L. A., L. M. Jones, and L. K. Hutton, The 1997 Southern California Seismic Network Bulletin, *Seismol. Res. Lett.*, *69*, 532–549, 1998.

Wyss, M., and S. Wiemer, Change in the probability for earthquakes in southern California due to the Landers magnitude 7.3 earthquake, *Science*, *290*, 1334–1338, 2000.

Ziv, A., and A. M. Rubin, Static stress transfer and earthquake triggering: No lower threshold in sight?, *J. Geophys. Res.*, *105*, 13,631–13,642, 2000.

P. Bodin, Center for Earthquake Research and Information, University of Memphis, 3876 Central Avenue, Memphis, TN 38152, USA. (bodin@ceri.memphis.edu)

J. Gomberg, U.S. Geological Survey, CERI, 3892 Central Avenue, Suite 2, Memphis, TN 38152, USA. (gomberg@usgs.gov)

D. Kilb, Institute for Geophysics and Planetary Physics, University of California, San Diego, MS 0225, La Jolla, CA 92093-0225, USA. (dkilb@epicenter.ucsd.edu)

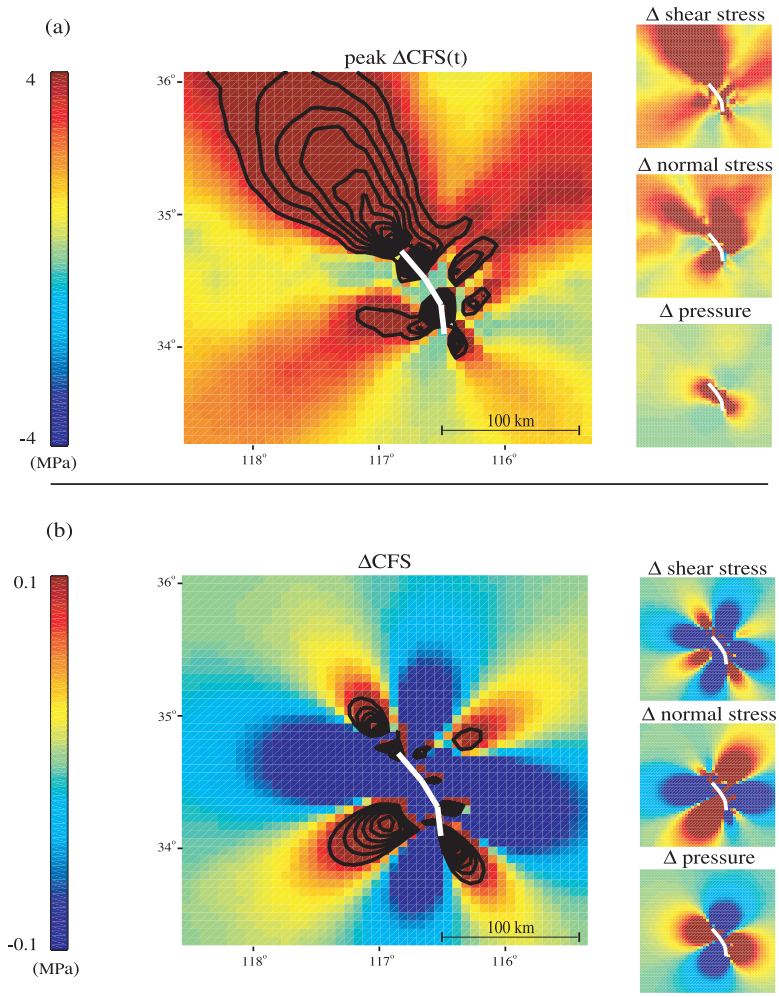


**Figure 5.** (a) Map at 4.5 km depth of peak $\Delta CFS(t)$ with contours indicating levels of peak $\Delta CFS(t) \geq 4$ MPa with equal intervals of 1.5 MPa. Peak $\Delta CFS(t)$ values are, by definition, always positive. Also shown are maps of the individual components that compose the final peak $\Delta CFS(t)$ map. (b) As in Figure 5a but for a map of $\Delta CFS$ with contours indicating levels of $\Delta CFS(t) \geq 0.1$ MPa with equal intervals of 0.05 MPa.